Redox Biol. 2019 Jun; 24: 101176. PMCID: PMC6438913
Published online 2019 Mar 23. doi: 10.1016/j.redox.2019.101176 PMID: 30921636

SELENON (SEPN1) protects skeletal muscle from saturated fatty acid-induced ER stress and insulin resistance

Ersilia Varone,[a,1] Diego Pozzer,[a,1] Simona Di Modica,[a] Alexander Chernorudskiy,[a] Leonardo Nogara,[b,c] Martina Baraldo,[b,c] Mario Cinquanta,[d] Stefano Fumagalli,[e] Rocio Nur Villar-Quiles,[f] Maria-Grazia De Simoni,[e] Bert Blaauw,[b,c] Ana Ferreiro,[f] and Ester Zito[a,*]

[a]Dulbecco Telethon Institute at Istituto di Ricerche Farmacologiche Mario Negri, IRCCS, Milan, Italy
[b]Department of Biomedical Sciences, University of Padua, Padua, Italy
[c]Venetian Institute of Molecular Medicine, Padua, Italy
[d]Cogentech Società Benefit srl, at IFOM, Via Adamello, Milan, Italy
[e]Istituto di Ricerche Farmacologiche Mario Negri, IRCCS, Milan, Italy
[f]Pathophysiology of Striated Muscles laboratory, Unit of Functional and Adaptive Biology, BFA, University Paris Diderot/CNRS, Sorbonne Paris Cité, Paris, France - AP-HP, Centre de Référence Maladies Neuromusculaires Paris-Est, Groupe Hospitalier Pitié-Salpêtrière, 75013, Paris, France
Ester Zito: ester.zito@marionegri.it
*Corresponding author. IRCCS-Istituto di Ricerche Farmacologiche Mario Negri, Via La Masa 19, 20156, Milano, Italy. ester.zito@marionegri.it
[1]These authors contributed equally to the study.

Received 2019 Feb 6; Revised 2019 Mar 4; Accepted 2019 Mar 20.

Abstract

Selenoprotein N (SELENON) is an endoplasmic reticulum (ER) protein whose loss of function leads to a congenital myopathy associated with insulin resistance (SEPN1-related myopathy). The exact cause of the insulin resistance in patients with SELENON loss of function is not known. Skeletal muscle is the main contributor to insulin-mediated glucose uptake, and a defect in this muscle-related mechanism triggers insulin resistance and glucose intolerance. We have studied the chain of events that connect the loss of SELENON with defects in insulin-mediated glucose uptake in muscle cells and the effects of this on muscle performance. Here, we show that saturated fatty acids are more lipotoxic in SELENON-devoid cells, and blunt the insulin-mediated glucose uptake of SELENON-devoid myotubes by increasing ER stress and mounting a maladaptive ER stress response. Furthermore, the hind limb skeletal muscles of SELENON KO mice fed a high-fat diet mirrors the features of saturated fatty acid-treated myotubes, and show signs of myopathy with a compromised force production. These findings suggest that the absence of SELENON together with a high-fat dietary regimen increases susceptibility to insulin resistance by triggering a chronic ER stress in skeletal muscle and muscle weakness.

Importantly, our findings suggest that environmental cues eliciting ER stress in skeletal muscle (such as a high-fat diet) affect the pathological phenotype of SEPN1-related myopathy and can therefore contribute to the assessment of prognosis beyond simple genotype-phenotype correlations.

Keywords: Insulin resistance, ER stress response, SELENON, SEPN1, Congenital myopathies

1. Introduction

SELENON is localised in the endoplasmic/sarcoplasmic reticulum (ER/SR), has a thioredoxin reductase-like domain on the ER side of its sequence, and regulates ER calcium levels by means of the redox regulating SERCA2 pump [[1], [2], [3]]. Despite its ubiquitous expression, SELENON loss of function gives rise to a selective muscle pathological phenotype associated with insulin resistance [4]. As the majority of insulin-dependent glucose uptake (75–90%) takes place in skeletal muscle, a defect in skeletal muscle insulin-dependent glucose disposal is widely viewed as being critical for the development of whole-body insulin resistance and type 2 diabetes [5].

Insulin signal transduction is activated in skeletal muscle following the binding of insulin to insulin receptor tyrosine kinase. The activated receptor phosphorylates the downstream docking protein substrates which, as a result of phosphatidylinositol 3-kinase and Akt pathway activation, leads to the translocation of the GLUT4 glucose transporter to the plasma membrane and cellular glucose uptake [6].

Long-chain saturated fatty acid accumulation is lipotoxic in skeletal muscle [7,8] and induces ER stress, the consequent ER stress response [9] that together with mitochondrial dysfunction contributes to the pathogenesis of the muscle insulin resistance by inhibiting glucose transport [[10], [11], [12]]. ER and mitochondria communicate through the mitochondria associated membranes (MAMs), the disruption of which also triggers insulin resistance by inducing ER stress and affecting mitochondrial metabolism [[13], [14], [15]].

We here show that the lack of SELENON in saturated fatty acid-challenged myotubes blunts insulin-dependent glucose uptake (i.e. triggers insulin resistance) by eliciting ER stress, disrupting ER-to-mitochondria communications, and altering mitochondria quality and cell bioenergetics. Importantly, SELENON KO mice fed a high-fat diet are more glucose intolerant, and their skeletal muscles show impaired insulin signalling, strength force, and an increased ER stress. A combination of SELENON loss and a high-fat diet therefore synergistically contribute to the pathogenesis of SEPN1-related myopathy by triggering insulin resistance and impairing muscle performance.

2. Results

2.1. Insulin resistance is part of the phenotype in SEPN1-related myopathy patients

Autosomal recessive mutations of the *SELENON* gene (also known as *SEPN1*) cause SEPN1-related myopathy, a rare congenital myopathy typically associated with low body mass index (BMI) [16]. Insulin resistance was first reported in 5 SEPN1-related myopathy patients in 2006 [4]. To confirm the association between SELENON defects and insulin resistance, we evaluated retrospectively follow-up data from eight patients with confirmed SELENON mutations in whom an oral glucose tolerance test (OGTT) had been performed. All patients had congenital muscle weakness more severe in axial muscles, respiratory insufficiency and scoliosis, typical of SEPN1-related myopathy. The results of the OGTT, summarized in Table 1, disclosed abnormal glucose metabolism in 4 of the 8 patients, despite a very low body mass index (<13.1). Patient 1 showed high level of fasting glycemia, without any increase in glycated hemoglobin. Patients 2–4 had normal basal glycemia but altered OGTT. Interestingly, Patient 1 evolved from normal fasting blood glucose and OGGT at age of 37 years to basal hyperglycemia one year later, stressing the need for regular controls of glucose metabolism

during the follow-up of SEPN1-related myopathy patients. There was no correlation between abnormal glucose metabolism and patient age or with the type of SELENON mutation (truncating, nonsense or missense). In contrast, insulin-resistance or prediabetes were observed only in patients with extremely low BMI values. These results confirm that paradoxical insulin resistance in very low BMI patients is part of the SEPN1-related myopathy phenotype.

Table 1

Patient	**1**	**2**	**3**	**4**	
Sex	M	F	F	F	M
Age years (y)	38	22	52	47	28
SELENON mutation	c.713dupA (p.N238Kfs*63) + c.1397G>A (p.R466Q)	c.713dupA (p.N238Kfs*63) homozygous	c.13_22dup (p.Q8Pfs*78) + c.883G>A (p.E295K)	c.13_22dup (p.Q8Pfs*78) homozygous	c.99 (p.V hom
FPG (mmol/L)	<6 at 37y **6.7** at 38y	4.8	4.6	4.9	<6
OGTT	Normal at 37y	Increased 2 h insulin concentration (61.2 mU/l)	Increased 1 h and 2 h plasma glucose (12.3 and 9.8 mmol/L). Increased 2 h insulin (37.74mU/L)	Increased 2 h plasma glucose (9.9 mmol/L)	Nor
BMI (kg/m^2)	11.7	12.8	13.1	13	18

Open in a separate window

F: female; M: male; FPG: Fasting plasma glucose (reference range: 4–6 mmol/L); OGTT: Oral glucose tolerance test (reference values: 1 h post-load plasma insulin <80 mU/L, 2 h post-load plasma insulin <14 mU/L, 1 h and 2 h post-load plasma glucose <10 mmol/L and <7.8 mmol/L respectively); BMI: Body Mass Index (reference values: <18.5:underweight; 18.5–24.9: healthy weight; 25–29.9: overweight; >30: obese). UK: unknown.

2.2. SELENON signal is clustered in response to a palmitate challenge

We moved to a cell system to study the chain of events that connect SELENON loss with an insulin resistant phenotype. In order to overcome the problems associated with unreliable SELENON antibodies, we used CRISPR/CAS9 technology to insert a green fluorescent protein (GFP) tag at the C-terminal of the *SelenoN* genomic locus of C2C12 myoblasts, and then selected and genomically sequenced the clones homozygous for the GFP insertion in order to prove the correct insertion (Fig. Sup 1–3). The relatively low fluorescent levels in the vehicle-treated cells indicated poor SELENON-GFP signal, but treatment with the saturated fatty acid palmitate (palm, 100 μM) increased the fluorescence of SELENON-GFP without significantly changing that of the KDEL protein ER markers (

Fig. 1A and B). In addition, the SELENON-GFP signal appeared clustered in granular signal rather than showing a more typical tubular ER pattern after palmitate treatment (Fig. 1C and D), thus indicating higher fluorescence and different spatial distribution of SELENON after palmitate.

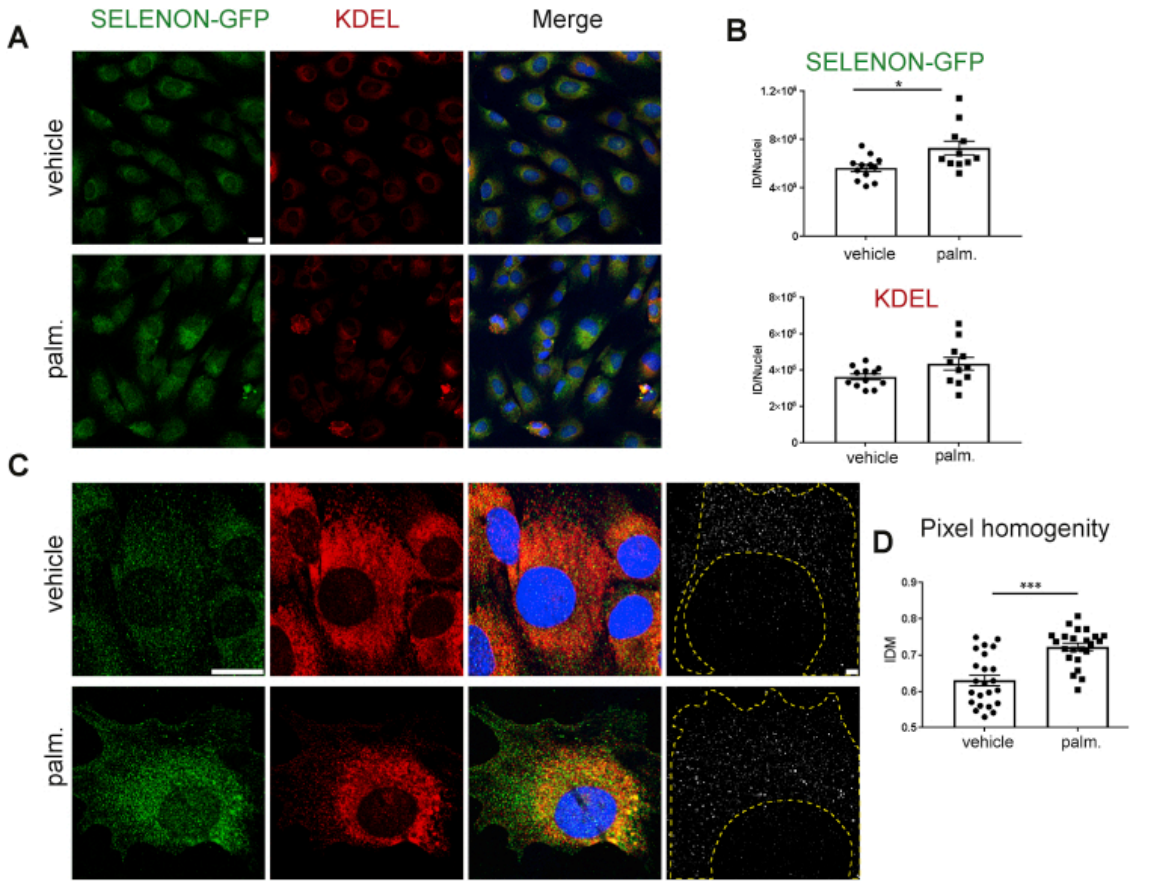

Open in a separate window

Fig. 1

Higher SELENON levels in palmitate-treated cells. A) Representative images of GFP immunofluorescence in confocal field of views analysed for vehicle-treated (upper panels) or (100 μM) palmitate-treated (lower panels) C2C12 showing SELENON-GFP signal. Nuclei are in blue, SELENON-GFP in green and KDEL (ER staining) in red. Scale bar 20 μm. B) The fluorescence intensity of SELENON-GFP is increased in palmitate treated cells while that of KDEL does not significantly change. Each dot represents one field of views. C) Representative 100× images of cells treated with vehicle (upper panels) or palmitate 100 μm (lower panels) showing SELENON-GFP clustering. Scale bar 20 μm. The panels on the right show the super-resolution image (SIM) of SELENON-GFP; scale bar 2 μm. D) Quantification of SELENON-GFP signal distribution using a gray-level co-occurrence matrix over the yellow outline of the SIM images revealed increased pixel homogeneity (expressed as inverse difference moment, IDM) in the palmitate-treated cells indicating greater signal clustering. Each dot represents one cell.

2.3. SELENON deficiency affects the ER and mitochondria

ER, mitochondria and MAM impairments are involved in the onset of insulin resistance [14,17,18]. In order to analyse the ER, mitochondria and MAMs of palmitate-treated SELENON Knock down (KD) C2C12 cells in detail, we used a combination of specific fluorescent trackers and super-resolution microscopy (Fig. Sup 4). Analysis of the fluorescence of the ER and mitochondria trackers in relation to cell area and their overlapping fluorescent signal showed that the palmitate treatment of SELENONKD cells shrunk the ER area fraction (WT versus SELENON KD and SELENON KD versus SELENON KD, palm.), reduced ER-to-mitochondria contacts (ER_{mito} Area fraction) (WT versus SELENON KD and SELENON KD versus SELENON KD, palm.) and reduced the total mitochondrial content (Total mito area fraction) (SELENON KD versus SELENON KD, palm.) (Fig. 2 A and B). In addition, an *ad hoc* skeletonised analysis of mitochondria morphology showed that palmitate triggered mitochondria fragmentation to a greater extent in SELENON KD cells than in wild-type (WT) cells (Fig. 2C and D). It is worth noting that the palmitate-treated SELENON KD cells had less ATP (Fig. 2E), thus suggesting that both the absence of SELENON and palmitate affect the ER and mitochondrial morphology and compromise cell bioenergetics.

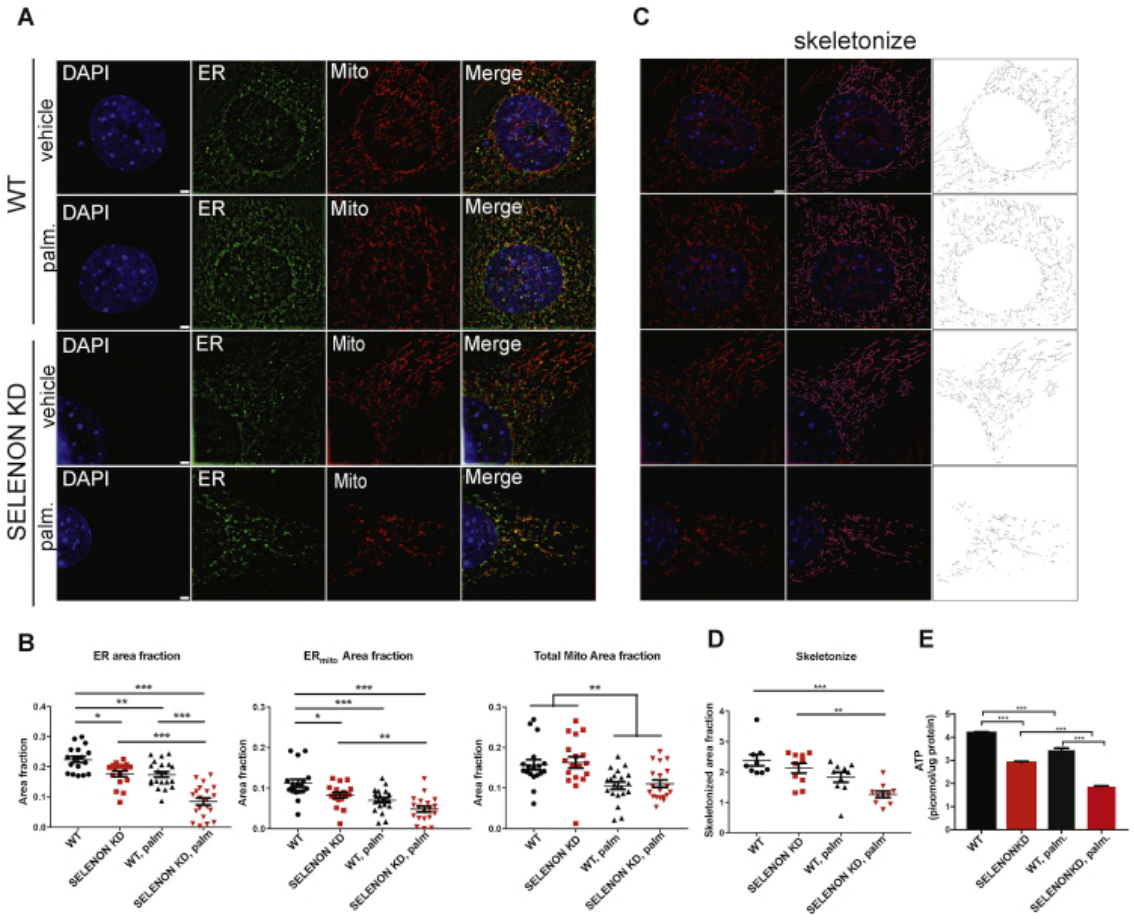

Open in a separate window

Fig. 2

The absence of SELENON and treatment with palmitate both impair ER and mitochondria. A) Representative SIM images of WT or SELENON KD C2C12 cells treated with vehicle or palmitate (palmitate was used at 100 μM) showing the nuclei (blue), ER (green) and mitochondria (red). Scale bar 2 μm. B) Dot plots representing the ER area fraction (i.e. the area occupied by the ER), the ER_{mito} area fraction (i.e. the mitochondrial signal closer to the ER) and the total mito area fraction (i.e. total mitochondrial signal). C) The mitochondria signal was segmented and skeletonised and the related area calculated. On the right, representation of the area occupied by the skeletonised mitochondria. D) Dot plots representing the skeletonised area fraction. Each dot represents one cell. E) Measurement of the cellular ATP content of WT and SELENON KD cells treated or not with palmitate (n = 4).

2.4. SELENON deficiency worsens palmitate-induced lipotoxicity by eliciting ER stress

As the presence of lipid droplets in skeletal muscle is associated with insulin resistance [19], we investigated the content of the lipid droplets in WT and SELENON KD C2C12 cells after treatment with vehicle or palmitate. The fluorescence levels of BODIPY (boron-dipyrromethene, a molecule that fluorescently stains neutral lipids) indicated that the content of the droplets in both WT and SELENON KD C2C12 cells was higher after palmitate treatment than after treatment with the vehicle alone, and higher in SELENON KD cells than in WT cells after both treatments (Fig. 3A and B).

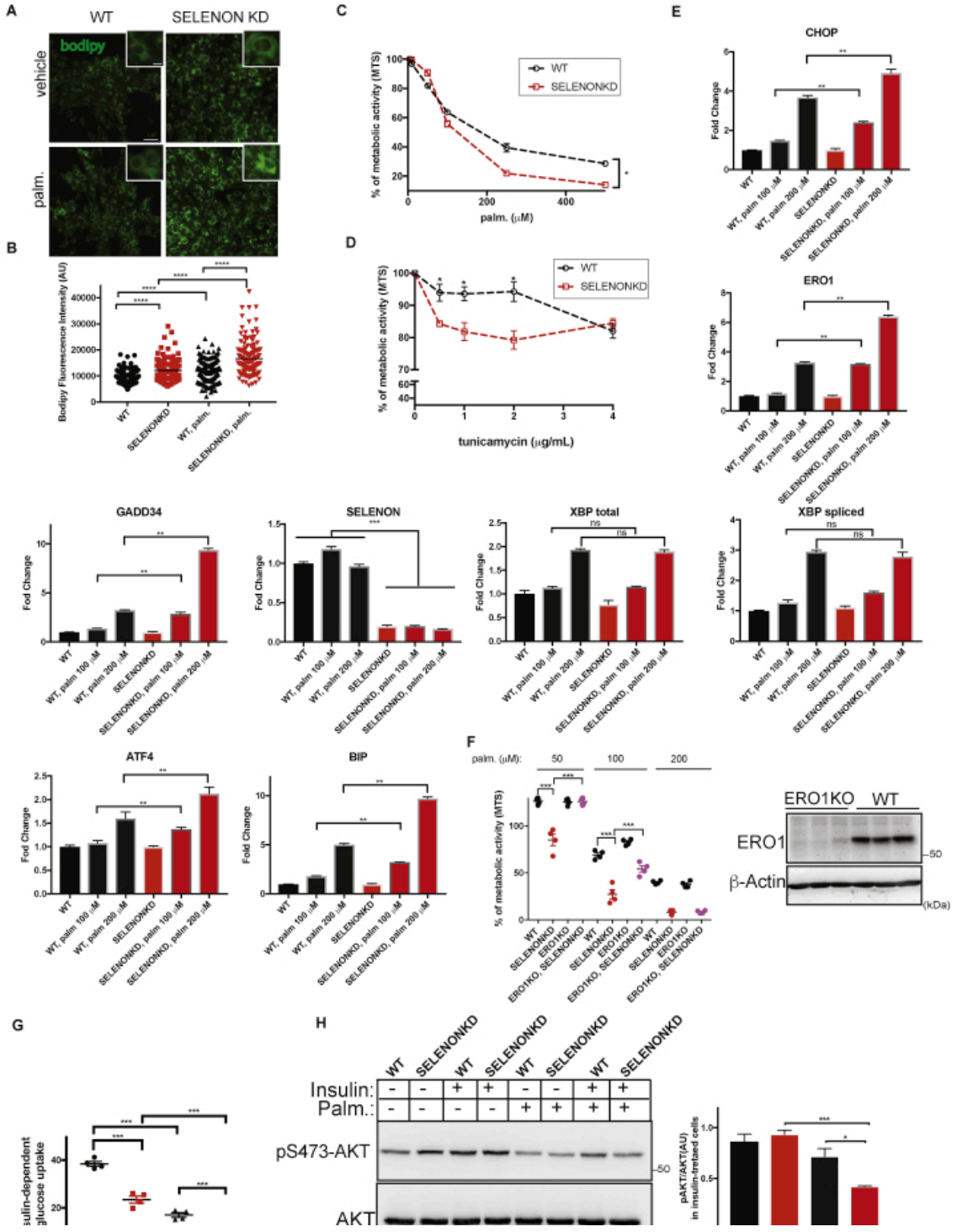

Open in a separate window

Fig. 3

Palmitate lipotoxicity is associated with ER stress and affects insulin signalling in SELENON KD myotubes. A) BODIPY staining of neutral lipids in vehicle- and palmitate-treated WT and SELENON KD C2C12 cells. Palmitate was used at 100 μM. Scale bar 50 μm and scale bar of the inset 10 μm. B) Quantification of BODIPY fluorescence (each dot represents one cell). C) Metabolic activity (MTS) of WT and SELENON KD C2C12 cells treated with the indicated concentrations of palmitate for 24 h. Metabolic activity is expressed as the relative reduction in MTS in palmitate-exposed cells in comparison with vehicle-treated cells (arbitrarily set at 100%) (n = 4). D) Metabolic activity (MTS) of WT and

SELENON KD C2C12 cells treated with the indicated concentrations of tunycamicin for 12 h. Metabolic activity is expressed as the relative reduction in MTS in tunycamicin-exposed cells in comparison with unexposed (DMSO-treated) cells (arbitrarily set at 100%) (n = 4). E) Semi-quantitative, real-time RT-PCR analysis of ER stress response markers in mRNA prepared from WT and SELENON KD C2C12 cells treated with BSA alone or 100 or 200 μM of palmitate (n = 3). F) Metabolic activity (MTS) of WT, ERO1KO, SELENON KD and ERO1KO, SELENONKD C2C12 cells treated with the indicated concentrations of palmitate for 24 h. Metabolic activity is expressed as the relative reduction in MTS in palmitate-exposed cells in comparison with vehicle-treated cells (arbitrarily set at 100%) (n = 4). Below, ERO1 and β-Actin Immunoblots of six different C2C12 clones after CRISPR/CAS9. Four of them (2WT and 2 ERO1KO) were treated with palmitate and analysed for metabolic activity. G) The dot plots indicate the insulin-mediated glucose uptake in vehicle- and palmitate-treated WT and SELENON KD C2C12 myotubes as a percentage of the increased glucose uptake after insulin treatment in comparison with basal glucose uptake in the same cells (n = 4). H) Representative immunoblots of *p*-AKT and AKT and, on the right, the relative quantification of the bands in arbitrary units (AU) in vehicle- and palmitate-treated WT and SELENON KD C2C12 myotubes. β-actin was used as a loading control (n = 3).

In order to assess whether lipid accumulation affects the metabolic rate of the cells, WT and SELENON KD C2C12 cells were exposed to palmitate at concentrations of 5–500 μM. MTS assays showed SELENON KD cells had lower metabolic rate than WT cells, which suggests the greater lipotoxicity of palmitate in SELENON KD cells (Fig. 3C). Similarly, the ER stressor tunicamycin used at concentrations of 0,5-4 μg/mL impaired the metabolic rate of SELENON KD C2C12 cells to a greater extent than that of WT cells (Fig. 3D), thus suggesting the greater susceptibility of SELENON KD cells to ER stress.

The absence of SELENON and treatment with palmitate both elicit ER stress [3,9,10,20,21], which in turn initiates an ancient multi-signalling pathway known as the ER stress response. The ER stress response usually promotes recovery from ER stress by inducing chaperones and attenuating protein translation by the IRE-1, ATF6 and PERK pathways. IRE-1 splices the mRNA of transcription factor X-box-binding protein 1 (XBP1spliced), which activates the transcription of ER stress response target genes; ATF6 promotes the induction of chaperone BIP; and PERK attenuates protein translation and up-regulates transcription factor ATF4. The PERK branch may also induce pro-apoptotic CHOP, the downstream protein disulfide oxidase ERO1 alpha (henceforth ERO1 [22]), and the phosphatase GADD34, which may be involved in a maladaptive ER stress response causing the failure of ER stress relief and dysfunction [23,24]. Interestingly, the IRE-1 and PERK branches of the ER stress response are also activated by lipotoxic stress due to saturated free fatty acid impairing membrane fluidity and promoting the dimerisation and activation of the IRE-1 and PERK pathways [9,25].

In order to determine whether the lower metabolic rate induced by palmitate in SELENON KD C2C12 cells is due to increased ER stress, we examined the levels of ER stress markers in WT and SELENON KD cells. Interestingly, the levels of BIP and ATF4 and all three maladaptive ER stress response mediators (CHOP, ERO1 and GADD34) were significantly higher in the SELENON KD cells treated with palmitate at two lipotoxic concentrations (100 and 200 μM) (Fig. 3E), thus indicating increased ER stress. Accordingly, the ablation of the maladaptive ERO1 (ERO1KO) in SELENON KD cells significantly increased the metabolic rate of these cells when compared to those with normal ERO1 levels and when the cells were treated with low concentrations of palmitate (50 and 100 μM) (Fig. 3F and Fig. Sup. 5).

2.5. SELENON deficiency impairs insulin-dependent glucose uptake

As ER stress may affect insulin-dependent glucose uptake [26], we investigated whether the lack of SELENON increases the susceptibility to insulin resistance of myotubes. To this end, WT and SELENON KD myotubes were tested for insulin-dependent glucose uptake in the presence of vehicle or palmitate (100 μM). As expected, metabolic tracings of ^{3}H-2 deoxy-glucose (2DG) showed that palmitate-treated WT and SELENON KD myotubes had reduced insulin-stimulated 2DG uptake in comparison with their vehicle-treated counterparts. Furthermore, uptake was less in the SELENON KD myotubes than in the WT, thus suggesting that palmitate and the lack of SELENON both contribute to the reduction (Fig. 3G).

Phosphorylation of AKT at Ser-473 triggers Glut4 translocation to the plasma membrane and glucose uptake [6]. In order to substantiate the finding of reduced insulin-dependent glucose uptake in palmitate-treated SELENON KD myotubes, we analysed AKT phosphorylation after insulin treatment. SELENON deficiency had no appreciable effect on the AKT phosphorylation of insulin-treated cells (lanes 3 versus 4 of Fig. 3H) but, together with palmitate treatment, it reduced AKT phosphorylation in comparison with the WT (lanes 7 versus 8 of Fig. 3H), suggesting impaired insulin signalling in palmitate-treated SELENON-devoid myotubes.

2.6. The ER stress inhibitor TUDCA partially rescues palmitate-induced lipotoxicity

In order to investigate whether relief from ER stress reduces palmitate-induced lipotoxicity in SELENON KD cells, we examined the effect of TUDCA, an inhibitor of ER stress [27]. To this end, WT and SELENON KD C2C12 cells were pre-conditioned with TUDCA 1 mM (a typical concentration in the literature [28]) for 12 h and then treated with palmitate (100 μM). The pre-conditioning led to a small but consistent improvement in MTS assay results (Fig. 4A) that suggested a higher metabolic rate in both palmitate-treated WT and SELENON KD cells.

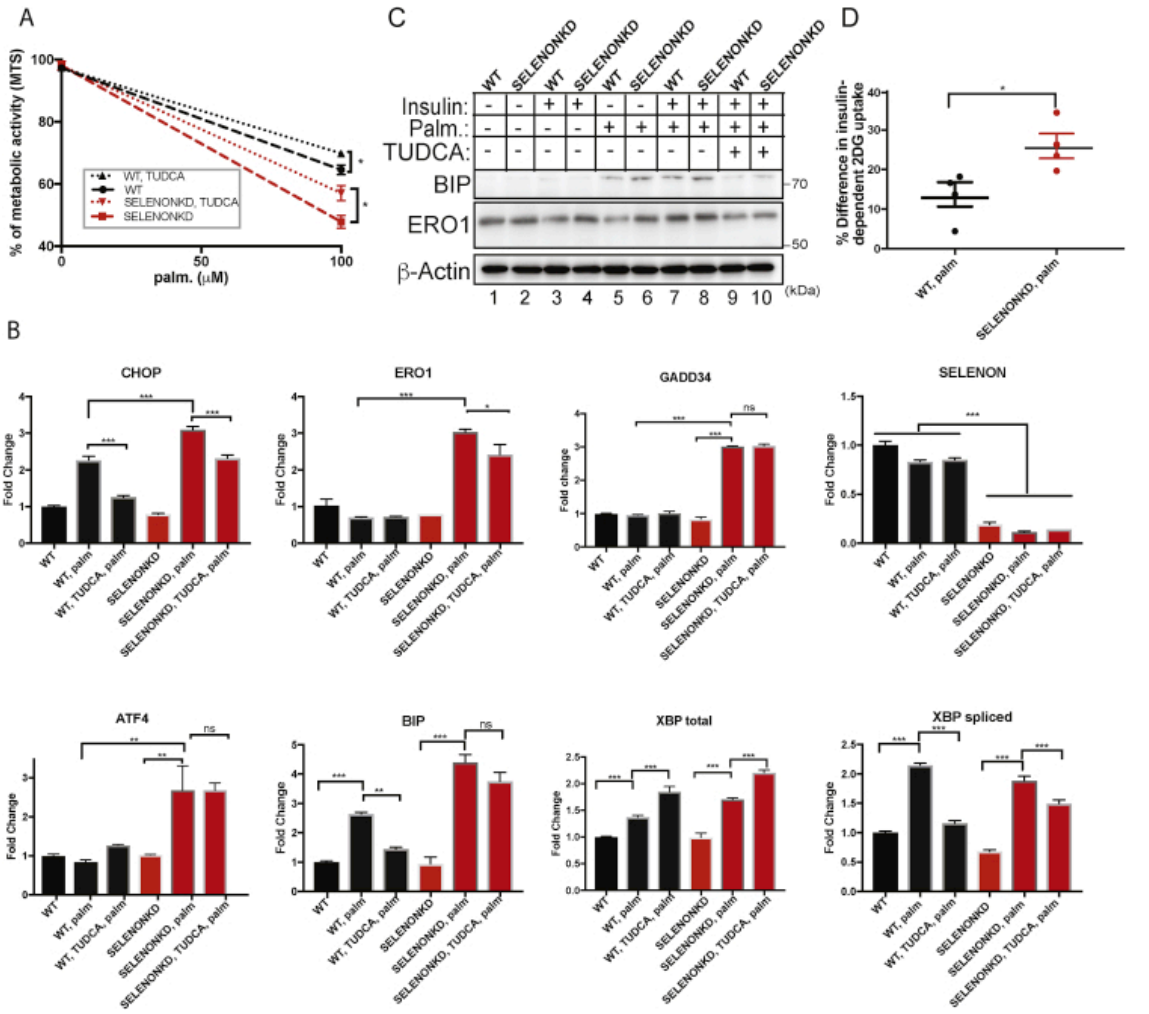

Open in a separate window

Fig. 4

TUDCA attenuates lipotoxicity and ER stress, and improves insulin-mediated glucose uptake in palmitate-treated myotubes. A) Metabolic activity (MTS) of WT and SELENON KD C2C12 cells pre-treated with TUDCA (1 mM) for 12 h, and then treated with palmitate for 24 h. Metabolic activity is expressed as the relative reduction in MTS in palmitate-treated cells in comparison with vehicle-treated cells (arbitrarily set at 100%) (n = 4). B) Semi-quantitative real-time RT-PCR analysis of ER stress response markers in mRNA prepared from WT and SELENON KD C2C12 cells treated with vehicle alone or palmitate 100 μM, or pretreated with TUDCA (1 mM) and then with palmitate 100 μM (n = 3). C) BIP, ERO1 and β-Actin Immunoblots of WT and SELENON KD C2C12 myotubes. D) Percentage improvement in insulin-mediated glucose uptake in WT and SELENON KD C2C12 myotubes pre-treated with TUDCA and then treated with palmitate in comparison with myotubes only treated with palmitate.

As expected, TUDCA reduced the levels of some ER stress response markers (CHOP, XBP spliced and BIP), but their levels were still higher in the SELENON KD than the WT myotubes. TUDCA pre-treatment also reduced the levels of the maladaptive response marker ERO1 in SELENON KD myotubes, thus indicating that it partially prevented ER stress and the consequent response (Fig. 4B). Accordingly, western blot analysis showed that TUDCA pre-treatment decreased the levels of BIP and ERO1 proteins in palmitate-treated WT and SELENON KD C2C12 cells (lanes 7 and 8 versus lanes 9

and 10 in Fig. 4C). It also increased insulin-stimulated 2DG uptake by 10% in the palmitate–treated WT cells, and by 30% in palmitate–treated SELENON KD cells (Fig. 4D), thus indicating that even the partial TUDCA-mediated prevention of palmitate-induced ER stress may limit lipotoxicity in WT and SELENON KD myotubes.

2.7. SELENON KO mice are more likely to develop glucose intolerance

In order to study the direct consequences of fatty acid-induced lipotoxicity on SELENON KO mouse metabolism and skeletal muscle, we fed 9-week-old adult male WT and SELENON KO mice a high-fat diet (40% of calories from fat) for nine weeks and compared them with their counterparts fed a standard diet.

The WT and SELENON KO mice fed the standard diet showed no statistically significant difference in weight gain, but the SELENON KO mice on the high-fat diet showed a tendency to gain less weight even though their food intake was similar to that of the WT mice (Fig. 5A).

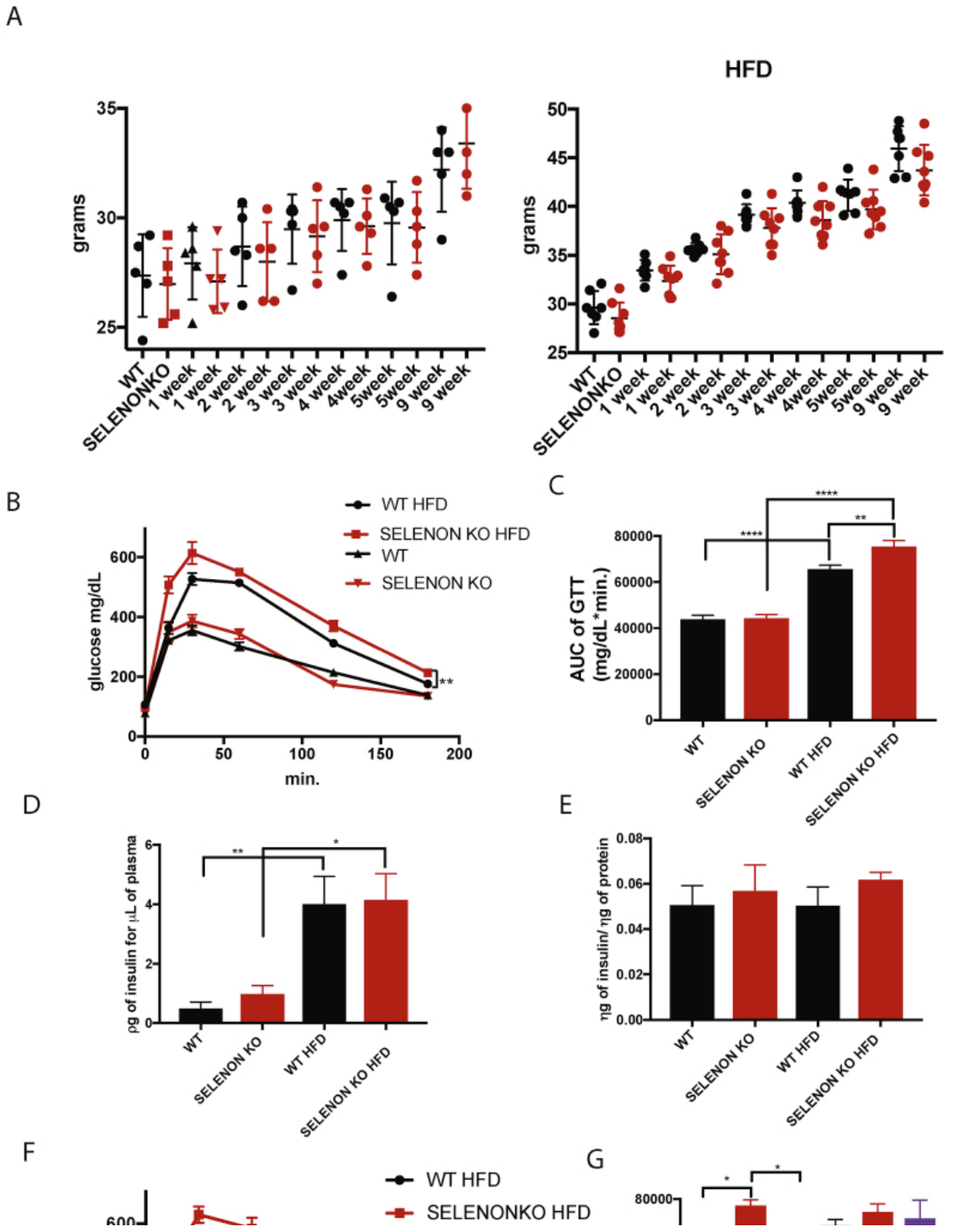

Open in a separate window

Fig. 5

SELENON loss affects glucose tolerance. A) Body weight of WT and SELENON KO mice fed a standard or high-fat diet (45% fat) for nine weeks (n = 5 on regular diet and n = 6 on HFD). B) Blood glucose concentrations after a glucose injection in WT and SELENON KO mice fed a standard or high-fat diet for nine weeks. C) Bar graphs showing the area under the curve (AUC) of the glycemic profile. D) Bar graphs showing plasma insulin levels. E) Bar graphs showing the levels of insulin extracted from the pancreas. F) Blood glucose concentrations after a glucose injection in WT, SELENON KO, CHOP KO and DKO

(SELENON and CHOP KO) mice fed a high-fat diet for six weeks. G) Bar graphs showing the area under the curve (AUC) of the glycemic profile of the mice with the indicated genotype fed a high-fat diet for six and eleven weeks (n = 6).

Glycemic control was comparable in the SELENON KO and WT mice on the standard diet (Fig. 5B) but, despite their lower weight gain after nine weeks on the high-fat diet, SELENON KO mice showed moderately greater glucose intolerance than the WT mice (Fig. 5B and C). This impaired glucose tolerance in comparison with the WT mice was not associated with a decrease in plasma and pancreas insulin levels but with a trend to an increase, thus suggesting that the defective glucose tolerance of the SELENON KO mice was not due to the lower levels of insulin secreted by the pancreas (Fig. 5D and E). Taken together, these findings suggest that SELENON loss in adult mice causes metabolic alterations such as glucose intolerance in response to a high-fat diet.

In order to investigate whether the glucose intolerance of SELENON KO mice on a high-fat diet improved in the absence of the maladaptive ER stress response mediator CHOP [29], we analysed WT, SELENON KO, CHOP KO and double SELENON/CHOP KO (DKO) mice fed a standard or high-fat diet. The deletion of CHOP improved the glucose tolerance of SELENON KO mice after six weeks on a high-fat diet, but the effect was only transient and completely disappeared after 11 weeks on the diet, possibly because CHOP deletion significantly increased obesity (Fig. 5F and G and Sup. 6).

2.8. SELENON KO and a high-fat diet impair insulin signalling and contractile performance in skeletal muscle

As AKT phosphorylation occurs downstream of insulin signalling [30] and is impaired in palmitate-treated SELENON KD myotubes, we analysed AKT phosphorylation in the gastrocnemius muscle of WT and SELENON KO mice fed a high-fat or standard diet. AKT was markedly phosphorylated in the muscles of the control WT mice fed a high-fat diet and much less so in the SELENON KO mice fed a high-fat diet (lanes 3–4 versus lanes 7–8 of Fig. 6A), thus indicating reduced insulin signalling in the muscle of the latter.

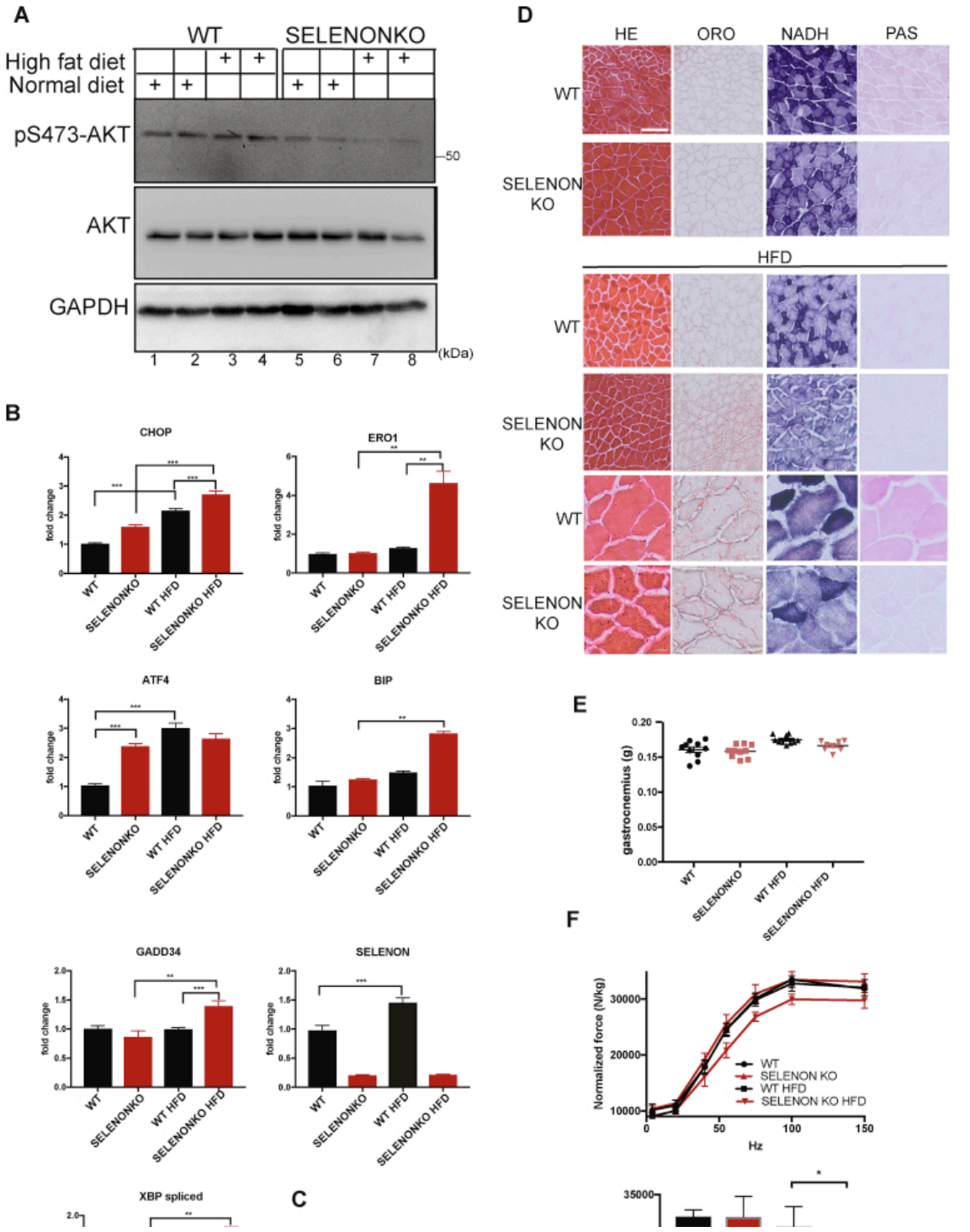

Open in a separate window

Fig. 6

SELENON loss impairs insulin signalling and muscle strength by increasing the ER stress response in skeletal muscle. A) Representative Immunoblots of *p*-AKT and AKT in the gastrocnemii of WT and SELENON KO mice fed a standard or high-fat diet. GAPDH was used as a loading control. B) Semi-quantitative, real-time RT-PCR analysis of ER stress response markers in mRNA prepared from gastrocnemii (n = 6). C) Real-time PCR quantification of the amount of gastrocnemius mtDNA in relation to that of RNase-P, a nuclear gene used as a standard (n = 6). The bar graphs represent the ratio between mitochondrial content in mice fed a high-fat and a standard diet. D) Representative HE, Oil Red O(ORO),

NADH and PAS micrographs of gastrocnemii (scale bar 40 μm). Below, high magnification micrographs (scale bar 20 μm). E) Dot plots representing the weight of each gastrocnemius. F) Force-frequency curves and bar graphs of the tetanic stimulation (stimulation frequency 100 Hz) representing the specific *in vivo* strength of the gastrocnemii (n = 6).

Subsequently, given the correlation between ER stress and insulin resistance, we analysed the levels of ER stress response markers in the gastrocnemius muscle. In qualitative agreement with our findings in palmitate-treated SELENON KD myotubes, the levels of the maladaptive response markers CHOP, ERO1 and GADD34 were higher in the gastrocnemii of the SELENON KO mice fed a high-fat diet, thus indicating an exacerbated maladaptive ER stress response (Fig. 6B). In addition, the small decrease in mitochondria content (Fig. 6C) indicated that, as in the case of the palmitate-treated C2C12 cells, the combination of a high-fat diet and SELENON loss leads to defects in the gastrocnemius that is not confined to the ER but also affects mitochondria. Despite these defects, the gastrocnemius of the SELENON KO mice fed a high-fat diet did not show any gross histological alterations in HE staining, but there was a substantial defect in NADH staining, more abundant in oxidative fibers, and in PAS staining indicating glycogen levels, which may have been due to impaired insulin signalling inhibiting glycogen synthase [31]. On the contrary, Oil Red O staining showed a sharp increase/accumulation in lipid droplets of high-fat-fed SELENON KO gastrocnemius (Fig. 6D). Despite the absence of muscle atrophy in the SELENON KO mice fed a high-fat diet in comparison with their counterparts fed a standard diet and the WT mice fed a high-fat diet (Fig. 6E), their muscles showed impaired normalised force. *In vivo* measurements of hind limb muscle force showed that the normalised muscle force of the gastrocnemius was similar in WT and SELENON KO mice on a standard diet, as has been previously shown [20], but force generation in the muscles of the SELENON KO mice fed a high-fat diet was significantly less during tetanic stimulation (100 Hz) (Fig. 6F), thus indicating that a high-fat dietary regimen and the lack of SELENON synergistically elicit ER stress, depress insulin signalling and impair force in skeletal muscle.

3. Discussion

SEPN1-related myopathy is a congenital muscular disorder arising from loss-of-function mutations in the SELENON gene [32,33]. Here, we show abnormalities in the glucose metabolism of patients with SEPN1-related myopathy that suggest insulin resistance. Interestingly, insulin resistance or prediabetes were observed only in patients with extremely low BMI values pointing to a correlation between severe reduction of the muscle and fat tissue and insulin resistance in SEPN1-related myopathy.

Skeletal muscle is the main contributor to post-prandial glucose uptake in the body, so defects in the availability of glucose in skeletal muscle impair metabolic flexibility and reduce body tolerance to glucose [34].

SELENON expression is responsive to ER stress [3] and impaired SELENON KO muscle shows greater ER stress and ER stress response [35], which can also be activated by the lipotoxic stress caused by a saturated fatty acid overload [9]. While eliciting ER stress and ER stress response, saturated fatty acid impairs insulin-dependent glucose uptake in myotubes [14] and a high-fat diet similarly induces ER stress in skeletal muscle and causes insulin resistance [36]. On the basis of these findings, we explored the hypothesis that SELENON deficiency sensitizes muscle cells to the consequences of ER stress and therefore increases the lipotoxicity of saturated fatty acids impairing insulin sensitivity.

Here we show that SELENON is induced during palmitate treatment of cells suggesting a function of SELENON during this treatment. The lack of SELENON during palmitate treatment not only alters ER homeostasis, but also reduces ER-mitochondria apposition (MAMs) and affects mitochondrial morphology and bioenergetics. Importantly, defects in MAMs and mitochondria are also linked to muscle insulin resistance [14,37].

A lack of SELENON increases palmitate-induced lipotoxicity as a result of fatty acid accumulation, thus eliciting ER stress, the consequent maladaptive ER stress response, and blunting insulin-dependent glucose uptake. Treatment with TUDCA, an ER stress inhibitor [27], reduced ER stress in palmitate-treated WT cells, but only slightly lowered the levels of ER stress response markers in palmitate–treated SELENON KD cells. However, surprisingly, it improved insulin-dependent glucose uptake in SELENON-devoid myotubes, clearly suggesting that ER stress is an important component of insulin resistance in SELENON mutant models.

SELENON deficiency triggers glucose intolerance in mice on a high-fat diet despite their trend towards gaining less weight than their WT counterparts. SELENON KO mice fed a high-fat diet show no overt abnormalities in plasma or pancreatic insulin content, suggesting that the glucose intolerance is not caused by a defect in endocrine pancreatic insulin secretion.

In qualitative agreement with findings in SELENON-devoid myotubes, SELENON deficiency impairs insulin signalling in skeletal muscle, as shown by reduced AKT phosphorylation, and leads to exaggerated ER stress, which suggests a correlation between reduced body glucose tolerance, insulin activity and increased ER stress in the muscles of SELENON KO mice fed a high-fat diet. These abnormalities in SELENON KO mice triggered by a high-fat diet reduce hind limb skeletal muscle strength, which is preserved in these mice fed a standard diet [3,20].

The expression of CHOP in SELENON KO muscle of high-fat-fed mice suggests that the maladaptive ER stress response contributes to the glucose intolerance, muscle insulin resistance and dysfunction. Previous studies have shown that the ablation of the maladaptive ER stress response mediator CHOP restores defective insulin secretion from pancreatic beta cells and glucose tolerance in mouse models of chronic ER stress [38,39]. However, CHOP ablation only temporarily rescues the glucose intolerance of SELENON KO mice fed a high-fat diet, suggesting that ER stress and the consequent response is involved in the phenotype of the insulin resistance of SELENON KO mutants, but also that chronic, ubiquitous ablation of CHOP has only a transient beneficial effect on the glucose tolerance and insulin resistance of SELENON KO models, probably as a result of some opposite effects: i.e. CHOP deletion increases obesity [40].

In brief, we propose a model in which the lack of SELENON sensitizes skeletal muscle to the consequences of chronic ER stress induced by palmitate treatment in cells or a high-fat diet in mice, thus impairing insulin signalling and affecting force-frequency responses in skeletal muscle. What is therapeutically important is that these findings suggest that environmental cues eliciting ER stress in skeletal muscle (such as a high-fat diet) affect the pathological phenotype of SEPN1-related myopathy, and can therefore contribute beyond simple genotype-phenotype correlations to establishing a prognosis.

Acknowledgments

The help of Marisa Aliprandi (Cogentech Società Benefit srl, Milan, Italy) for the CRISPR/CAS9-mediated GFP knock-in development is gratefully acknowledged.

This study was supported by a Telethon career award (TDEZ00112T), Italy, an ERC Cariplo grant (2014-1856), a Cariplo biomedical science for young scientist grant (2014-1075), an AIRC grant (MFAG 20018), Italy and a Cure CMD grant to EZ and a STARS consolidator grant, AFM-Téléthon,

France grant (21865) to BB.

Footnotes

Appendix A Supplementary data to this article can be found online at https://doi.org/10.1016/j.redox.2019.101176.

EXPERIMENTAL PROCEDURES

SELENON-related myopathy patients

Patients 1–8, of French origin, were included in a retrospective study of SEPN1-related myopathy natural history after diagnostic identification of *SELENON* mutations using genomic DNA, following previously described methods [16] and after informed consent according to local ethical committees. The variants were reported according to Human Genome Variation Society recommendations (http://varnomen.hgvs.org/) using the complete *SELENON* transcript as reference (NM_020451.2). Exons were numbered 1–13 according to the Locus Reference Genomic (LRG) schema.

Two-hour 75 g-Oral Glucose Tolerance Test (OGTT) was performed in all patients assessing fasting plasma glucose, insulin and C-Peptide as well as 1-h and 2-h post-load plasma glucose and insulin concentration.

Animal experiments

All of the procedures involving animals and their care carried out at the Mario Negri Institute and the University of Padua were conducted as described by their institutional guidelines, which are in accordance with national (D.L. no. 116, G.U. suppl. 40, Feb. 18, 1992, No.8, G.U., 14 luglio 1994) and international laws and policies (EEC Council Directive 86/609, OJ L 358, 1 DEC.12,1987; NIH Guide for the Care and use of Laboratory Animals, U.S. National Research Council, 1996) and the ARRIVE guidelines. The SELENON KO mice were purchased from the EMMA repository (SELENON<tm1.2Mred>/Orl) and the CHOP KO mice [29] (Stock No. 005530) from Jackson Laboratory. Male WT and SELENON KO mice were fed a regular diet or a high-fat diet (HFD) (MD. 88137, 42% from fat prepared by ENVIGO).

CHOP mice were crossed to SELENON KO mice, and male carriers of *Chop* deletion and discordant for the S*elenoN* deletion were evaluated.

Glucose Tolerance Test (GTT)

After an overnight starvation, the mice were intraperitoneally injected with 2 mg/g glucose (Merck) and basal blood glucose levels were measured from tail vein blood.

Insulin measurements

Plasma insulin levels were measured by means of an enzyme-linked immunosorbent assay (ELISA) (Abcam, ab100578) using mouse insulin as the standard. The pancreata were removed and immediately frozen in liquid nitrogen. Protein extracts were prepared using the acid/ethanol method. After neutralisation, the insulin in the extracts was measured by means of an ELISA (Abcam, ab100578). The protein in tissue extracts was determined using the Bradford method.

Construction and validation of the CRISPR/Cas9 plasmid for GFP knock-in at the C- terminal of the murine *Selenon (SepN1)* gene

We generated the GFP knock-in at the C-terminal of the *SelenoN (SepN1)* locus of C2C12 cells by means of CRISPR/Cas9-mediated homologous recombination (HDR) with a donor plasmid vector. The clones that were homozygous for the GFP insertion were selected by means of sequencing (as shown in Sup. Fig. 1, Fig. 2, Fig. 3).

ERO1 KO C2C12 cells

ERO1 KO C2C12 and the counterpart ERO1 WT C2C12 cells were generated with the CRISPR/CAS9 technology (sc-401747 and sc-401747-HDR, Santa Cruz Biotechnology), closely following the manufacturer's instructions. The clones were selected in 6 μg/mL of puromycin and twenty of them analysed for ERO1 levels by Immunoblot.

SELENON KD recombinant adenovirus

The SELENON shRNA sequence TRCN0000247860 was sub-cloned under a U6 promoter together a GFP under a CMV promoter in an adenoviral-Type5 (dE1/E3) backbone and the adenovirus was produced by Vector BIOLABS (Malvern, PA, USA) (titer 2.7×10^{10} PFU/mL). Similarly, a GFP adenovirus (Ad-CMV-GFP, titer 1×10^{10} PFU/mL) was produced as a control. The adenoviruses were used at 200 multiplicity of infection (MOI) to infect low passages C2C12 cells at a 50% of confluence in differentiation media (DMEM high glucose, 5% horse serum). After 3 days in differentiation media the cells were harvested and the levels of SELENON were analysed by Real-Time quantitative PCR. After additional three days of differentiation (six days of differentiation) glucose uptake was assessed. Given the presence of GFP (which interferes with BODIPY fluorescence), the experiment whose results are shown in Fig. 3A was carried using SELENON shRNA TRCN0000247860-encoding lentivirus [3,20].

MTS assay

Six thousand C2C12 cells/well were plated in 96-well plates. A day later, the media was replaced and the cells incubated with complete media with or without TUDCA for 16 h and then the media was changed again and the cells incubated with tunicamycin (12 h) or palmitate (24 h). Later cells were incubated in MTS [3-(4,5-dimetiltiazolo-2-il)-5-(3-carbossimetossifenil)-2-(4-solfofenil)-2H-tetrazolio] and PMS (Phenazine methosulfate) as indicated in CellTiter 96® Aqueous Non-Radioactive Cell Proliferation Assay (Promega). Acquisitions were made by TECAN infinite M200 using excitation wavelengths at 490 nm.

Lipid Droplets detection by BODIPY 493/503 staining for microscopy

Cells were incubated with 2 μM Bodipy (1987239, Invitrogen) and 5 μM Hoechst in DMEM media with 0,25% FBS in a cell culture incubator for 20 min and then fixed with 4% formalin. Slides are imaged immediately by acquiring six non-overlapping 621 × 621 μm fields per well randomly. Acquisitions were made by microscopy (Virtual slide microscope BX6-VS, Olympus) using excitation wavelengths at 488 nm. Unsaturated 1937 × 1937 pixel images were acquired with a 20× objective. After proper background subtraction, 150 cells were selected with manual tracing and fluorescent signal was quantified by ImageJ software as mean gray level value per cell.

TUDCA, palmitate, tunicamycin treatment

C2C12 were incubated with palmitic acid (P0500 SIGMA), that was previously conjugated with fatty-acid free BSA, for 24 h and compared with vehicle (BSA)-treated cells or with tunicamycin (T7765, SIGMA) for 12 h and compared with DMSO-threated cells. C2C12 were pretreated with TUDCA (580549, MIliipore) at 1 mM or PBS for 16 h to evaluate ER stress.

Glucose uptake measurement

C2C12 myotubes were serum starved for 1 h then incubated in Krebs-Ringer buffer (MgCl2: 0,0468 g/L, KCl: 0,34 g/L, Na2HPO4:0,1 g/L, NaH2PO4:0,18 g/L) with 0,3%BSA and with 0,5 μmol/L 2-deoxy-[3H]-D-glucose (4 μci/mL) for 30 min. Incubations were performed with or without insulin stimulation (30 min, 100 nM). After incubation, the medium was removed and cells were rapidly washed with cold Krebs-Ringer buffer, prior to lysis in 0,2%SDS. Cell content radioactivity was determined by liquid scintillation counting (Perkin Elmer 2800 TR, Courtaboeuf, France) and protein content was quantified by using the Bradford protein assay.

Mitochondria DNA quantification

Total DNA was extracted from muscles following standard isopropanol precipitation. For mtDNA content analysis, SYBR-GREEN real-time PCR was used with primers specific for a mouse mtDNA fragment of the cytochrome C oxidase 1 gene (F: TGCTAGCCGCAGGCATTACT R: CGGGATCAAAGAAAGTTGTGTTT), and primers specific to RNaseP (F: GCCTACACTGGAGTCCGTGCTACT R: CTGACCACACACGAGCTGGTAGAA), a single copy gene taken as a nuclear gene reference. Relative copy number was calculated using the ΔΔCt method.

ATP content

Cellular ATP content was determined using the ATP Determination kit (Molecular Probes; emission 560 nm at pH 7.8) as per the manufacturer's instruction manual (Thermo Fisher Scientific). Readings were normalised to protein concentration.

Confocal microscopy and quantitative analysis

Images for SELENON-GFP and KDEL were done by acquiring six non overlapping 274 × 274 μm fields per well randomly. Acquisitions were made by confocal microscopy (A1 scanning unit by Nikon, managed by software 'NIS-elements') using excitation wavelengths: 405 nm (nuclei), 488 nm (SELENON-GFP) and 561 nm (KDEL). Unsaturated 1024 × 1024 pixel images were acquired with a 20× objective, 0.5 NA, with Nyquist modality. To avoid bleed-through effects, a sequential scanning mode was used. After proper background subtraction and clearing the nuclear weak fluorescence observed in the SELENON-GFP channel, fluorescent signal for SELENON-GFP and KDEL (Fig. 1) was quantified by ImageJ software as integrated density (sum of all the gray-values present in the field of view) and normalised on the number of nuclei present in the quantified area. Representative confocal images of individual cells were obtained with a 100×1.49 NA oil immersion objective using the same laser excitation wavelengths. Graphic final elaboration of images was done by GIMP software.

Super resolution microscopy

Structured illumination microscopy (SIM) was done on a Nikon SIM system with a 100×1.49 NA oil immersion objective, managed by NIS elements software. Fourteen-bit images sized 1024 × 1024 pixels with a single pixel of 0.030 μm were acquired in a gray level range of 0–4000 to exploit the linear range of the camera (iXon ultra DU-897U, Andor) at 14-bit and to avoid saturation. Raw and reconstructed images were validated with the SIM check plugin of ImageJ [41]. ER (ER-Tracker Red) and mito (MitoTracker Deep Red) trackers were purchased from Molecular probes. Cells were randomly selected throughout the wells and imaged at laser excitation of 405 nm (nuclei), 488 nm (SELENON-GFP), 561 nm (KDEL or ER) and 640 nm (mitochondria) with a 3D-SIM acquisition protocol. SIM images were quantified with ImageJ. For the analysis of SELENON-GFP signal distribution, SIM images were converted to 8-bit and a region of interest was manually traced including the cell cytoplasm but not the nucleous. After background normalization pixel homogeneity was

quantified by the gray-level co-occurrence matrix (GLCM) analysis, done on the SELENON-GFP signal within the traced area with the ImageJ plugin 'GLCM analysis' (using step size = 1 pixel, step direction = 0°) (Fig. 1). Pixel homogeneity was expressed as inverse difference moment (IDM) [42]. For the quantification of ER and mitochondrial signals (Fig. 2), transfected cells were selected based on their GFP expression and a region of interest was manually traced including the cell cytoplasm but not the nucleous. After background normalization, the ER was segmentated by an automatic algorithm appropriately set up. The segmented ER was used to calculate the ER area (fraction of total cell area) and to obtain a mask to be applied to the mitochondrial signal. The mitochondrial signal was segmented by an automatic algorithm and the area present inside the ER mask was calculated as the fraction of total cell area and used for statistics. The segmentated mitochondrial signal was then followed by the skeletonize function to calculate the area of the skeletonised objects (fraction of total cell area). Graphic final elaboration of images was done by GIMP software.

Muscle analysis

The muscles were frozen in liquid nitrogen-cooled isopentane and fixed in formalin for morphological analysis, and cross-sections (8 μm) of isopentane-frozen muscle were stained with hematoxylin and eosin (HE) for histological analysis, with NADH-TR staining for the oxidative fiber content, PAS (Periodic Acid Schiff solution) staining for the glycogen content and oil red O staining for the lipid content.

Limb muscle force

In vivo hind limb muscle force was assessed as in Refs. [20,35].

Real-time quantitative RT-PCR analysis

Total RNA was isolated from the cells and muscle tissue using the RNeasy Mini Kit (Qiagen) in accordance with the manufacturer's instructions. One microgram of total RNA was reverse-transcribed and analysed using the Applied Biosystems' real-time PCR System and the ΔΔCt method. Relative gene expression in cells was normalised to beta-actin or cyclophilin, and relative gene expression in muscle was normalised to cyclophilin mRNA levels.

The real-time primers were:

mGADD34 F: GAGGGACGCCCACAACTTC R: TTACCAGAGACAGGGGTAGGT
mCHOP F: CCACCACACCTGAAAGCAGAA R: AGGTGAAAGGCAGGGACTCA
mBIP F: TCATCGGACGCACTTGGAA R: CAACCACCTTGAATGGCAAGA
mATF4 F: ATGGCCGGCTATGGATGAT R: CGAAGTCAAACTCTTTCAGATCCATT
mERO1 F: CATACTCAGCATCGGGGGAC R: GAATGTGAGCAAGCTGAGCG
mSELENON F: GCTTTCCTGTAGAGATGATG R:GCCCCGCCGGAGTCCTTC
mXBP1s F: GAGTCCGCAGCAGGTG R: GTGTCAGAGTCCATGGGA
mXBP1 total F: GGAGTGGAGTAAGGCTGGTG R: CCAGAATGCCCAAAGGATA

Antibodies

The following antibodies were used: mouse anti-beta Actin from Santa Cruz, mouse anti-GAPDH from Sigma, rabbit anti-phospho-Ser473 Akt (#4060, Cell Signalling Technology) and anti-Akt (#4691, Cell Signalling Technology), rabbit anti ERO1 [43] and mouse anti KDEL (ADI-SPA-827D, Enzo life Sciences).

Statistics

All data represent mean ± SEM and were analysed using Prism 6 software (Graphpad). An unpaired *t*-test was used for the two-group analyses (Fig. 1), and a one-way ANOVA multiple comparison test was used for the analysis of three or more groups (Fig. 2, Fig. 3, Fig. 4, Fig. 5, Fig. 6), two-way ANOVA for GTT tests in Fig. 5B and F and Fig.3C. One asterisk was used for $p < 0.05$, two for $p < 0.01$, three for $p < 0.001$, and four for $p < 0.0001$.

Appendix A. Supplementary data

The following are the Supplementary data to this article:

Supplementary Fig. 1–3. CRISPR/CAS9-mediated GFP knock-in at the C-terminal of the *SelenoN* locus of C2C12 cells.

Supplementary Fig. 4. Representative fluorescent micrographs representing C2C12 cells infected with a GFP or SELENON SHRNA adenovirus containing also a GFP under a CMV promoter. DAPI stains the nuclei. GFP positive cells were selected for microscopic studies.

Supplementary Fig. 5. Semi-quantitative, real-time RT-PCR analysis of ER stress response markers in mRNA prepared from C2C12 (n = 3).

Supplementary Fig. 6. Changes in the body weight of WT, SELENON KO, CHOP KO and SELENON, CHOP KO (DKO) mice fed a standard or high-fat diet (45% fat) for 11 weeks (n = 6).

Multimedia component 1:

Click here to view.(1.2M, pdf)Multimedia component 1

Multimedia component 2:

Click here to view.(7.8M, pdf)Multimedia component 2

Multimedia component 3:

Click here to view.(876K, pdf)Multimedia component 3

Multimedia component 4:

Click here to view.(830K, pdf)Multimedia component 4

References

1. Petit N., Lescure A., Rederstorff M., Krol A., Moghadaszadeh B., Wewer U.M. Selenoprotein N: an endoplasmic reticulum glycoprotein with an early developmental expression pattern. Hum. Mol. Genet. 2003;12(9):1045–1053. Epub 2003/04/18. PubMed PMID: 12700173. [PubMed] [Google Scholar]

2. Pitts M.W., Hoffmann P.R. Endoplasmic reticulum-resident selenoproteins as regulators of calcium signaling and homeostasis. Cell Calcium. 2017 PubMed PMID: 28506443; PubMed Central PMCID: PMCPMC5671369. [PMC free article] [PubMed] [Google Scholar]

3. Marino M., Stoilova T., Giorgi C., Bachi A., Cattaneo A., Auricchio A. SEPN1, an endoplasmic reticulum-localized selenoprotein linked to skeletal muscle pathology, counteracts hyper-oxidation by means of redox-regulating SERCA2 pump activity. Hum. Mol. Genet. 2015;24:1843–1855. Epub 2014/12/03. doi: ddu602 [pii] 10.1093/hmg/ddu602. PubMed PMID: 25452428. [PubMed] [Google Scholar]

4. Clarke N.F., Kidson W., Quijano-Roy S., Estournet B., Ferreiro A., Guicheney P. SEPN1: associated with congenital fiber-type disproportion and insulin resistance. Ann. Neurol. 2006;59(3):546–552. Epub 2005/12/21, PubMed PMID: 16365872. [PubMed] [Google Scholar]

5. Abdul-Ghani M.A., DeFronzo R.A. Pathogenesis of insulin resistance in skeletal muscle. J. Biomed. Biotechnol. 2010;2010:476279. PubMed PMID: 20445742; PubMed Central PMCID: PMCPMC2860140. [PMC free article] [PubMed] [Google Scholar]

6. Herman M.A., Kahn B.B. Glucose transport and sensing in the maintenance of glucose homeostasis and metabolic harmony. J. Clin. Investig. 2006;116(7):1767–1775. PubMed PMID: 16823474; PubMed Central PMCID: PMCPMC1483149. [PMC free article] [PubMed] [Google Scholar]

7. Turpin S.M., Lancaster G.I., Darby I., Febbraio M.A., Watt M.J. Apoptosis in skeletal muscle myotubes is induced by ceramides and is positively related to insulin resistance. Am. J. Physiol. Endocrinol. Metab. 2006;291(6):E1341–E1350. PubMed PMID: 16849630. [PubMed] [Google Scholar]

8. Samuel V.T., Shulman G.I. Mechanisms for insulin resistance: common threads and missing links. Cell. 2012;148(5):852–871. PubMed PMID: 22385956; PubMed Central PMCID: PMCPMC3294420. [PMC free article] [PubMed] [Google Scholar]

9. Volmer R., Ron D. Lipid-dependent regulation of the unfolded protein response. Curr. Opin. Cell Biol. 2015;33:67–73. PubMed PMID: 25543896; PubMed Central PMCID: PMCPMC4376399. [PMC free article] [PubMed] [Google Scholar]

10. Flamment M., Hajduch E., Ferre P., Foufelle F. New insights into ER stress-induced insulin resistance. Trends Endocrinol. Metabol. 2012;23(8):381–390. PubMed PMID: 22770719. [PubMed] [Google Scholar]

11. Patti M.E., Corvera S. The role of mitochondria in the pathogenesis of type 2 diabetes. Endocr. Rev. 2010;31(3):364–395. PubMed PMID: 20156986; PubMed Central PMCID: PMCPMC3365846. [PMC free article] [PubMed] [Google Scholar]

12. Randle P.J., Garland P.B., Hales C.N., Newsholme E.A. The glucose fatty-acid cycle. Its role in insulin sensitivity and the metabolic disturbances of diabetes mellitus. Lancet. 1963;1(7285):785–789. PubMed PMID: 13990765. [PubMed] [Google Scholar]

13. Sebastian D., Hernandez-Alvarez M.I., Segales J., Sorianello E., Munoz J.P., Sala D. Mitofusin 2 (Mfn2) links mitochondrial and endoplasmic reticulum function with insulin signaling and is essential for normal glucose homeostasis. Proc. Natl. Acad. Sci. U. S. A. 2012;109(14):5523–5528. PubMed PMID: 22427360; PubMed Central PMCID: PMCPMC3325712. [PMC free article] [PubMed] [Google Scholar]

14. Tubbs E., Chanon S., Robert M., Bendridi N., Bidaux G., Chauvin M.A. Disruption of mitochondria-associated endoplasmic reticulum membrane (MAM) integrity contributes to muscle insulin resistance in mice and humans. Diabetes. 2018;67(4):636–650. PubMed PMID: 29326365.

[PubMed] [Google Scholar]

15. Chernorudskiy A.L., Zito E. Regulation of calcium homeostasis by ER redox: a close-up of the ER/mitochondria connection. J. Mol. Biol. 2017;429(5):620–632. Epub 2017/02/01, PubMed PMID: 28137421. [PubMed] [Google Scholar]

16. Ferreiro A., Quijano-Roy S., Pichereau C., Moghadaszadeh B., Goemans N., Bonnemann C. Mutations of the selenoprotein N gene, which is implicated in rigid spine muscular dystrophy, cause the classical phenotype of multiminicore disease: reassessing the nosology of early-onset myopathies. Am. J. Hum. Genet. 2002;71(4):[739]–[749]. Epub 2002/08/23. doi: S0002-9297(07)60361-9 [pii] 10.1086/342719. PubMed PMID: 12192640; PubMed Central PMCID: PMC378532. [PMC free article] [PubMed] [Google Scholar]

17. Arruda A.P., Pers B.M., Parlakgul G., Guney E., Inouye K., Hotamisligil G.S. Chronic enrichment of hepatic endoplasmic reticulum-mitochondria contact leads to mitochondrial dysfunction in obesity. Nat. Med. 2014;20(12):1427–1435. PubMed PMID: 25419710; PubMed Central PMCID: PMCPMC4412031. [PMC free article] [PubMed] [Google Scholar]

18. Tubbs E., Theurey P., Vial G., Bendridi N., Bravard A., Chauvin M.A. Mitochondria-associated endoplasmic reticulum membrane (MAM) integrity is required for insulin signaling and is implicated in hepatic insulin resistance. Diabetes. 2014;63(10):3279–3294. PubMed PMID: 24947355. [PubMed] [Google Scholar]

19. Unger R.H., Scherer P.E. Gluttony, sloth and the metabolic syndrome: a roadmap to lipotoxicity. Trends Endocrinol. Metabol. 2010;21(6):345–352. PubMed PMID: 20223680; PubMed Central PMCID: PMCPMC2880185. [PMC free article] [PubMed] [Google Scholar]

20. Pozzer D., Favellato M., Bolis M., Invernizzi R.W., Solagna F., Blaauw B. Endoplasmic reticulum oxidative stress triggers tgf-beta-dependent muscle dysfunction by accelerating ascorbic acid turnover. Sci. Rep. 2017;7:40993. Epub 2017/01/21. doi: srep40993 [pii] 10.1038/srep40993. PubMed PMID: 28106121. [PMC free article] [PubMed] [Google Scholar]

21. Peter A., Weigert C., Staiger H., Machicao F., Schick F., Machann J. Individual stearoyl-coa desaturase 1 expression modulates endoplasmic reticulum stress and inflammation in human myotubes and is associated with skeletal muscle lipid storage and insulin sensitivity in vivo. Diabetes. 2009;58(8):1757–1765. PubMed PMID: 19478146; PubMed Central PMCID: PMCPMC2712792. [PMC free article] [PubMed] [Google Scholar]

22. Zito E. ERO1: a protein disulfide oxidase and H2O2 producer. Free Radic. Biol. Med. 2015;83: [299]–[304]. Epub 2015/02/06. doi: S0891-5849(15)00018-[0] [pii] 10.1016/j.freeradbiomed.2015.01.011. PubMed PMID: 25651816. [PubMed] [Google Scholar]

23. Ron D., Walter P. Signal integration in the endoplasmic reticulum unfolded protein response. Nat. Rev. Mol. Cell Biol. 2007;8(7):[519]–[529]. Epub 2007/06/15. doi: nrm2199 [pii] 10.1038/nrm2199. PubMed PMID: 17565364. [PubMed] [Google Scholar]

24. Marciniak S.J., Yun C.Y., Oyadomari S., Novoa I., Zhang Y., Jungreis R. CHOP induces death by promoting protein synthesis and oxidation in the stressed endoplasmic reticulum. Genes Dev. 2004;18(24):3066–3077. Epub 2004/12/17. doi: 18/24/3066 [pii] 10.1101/gad.1250704. PubMed PMID: 15601821; PubMed Central PMCID: PMC535917. [PMC free article] [PubMed] [Google Scholar]

25. Halbleib K., Pesek K., Covino R., Hofbauer H.F., Wunnicke D., Hanelt I. Activation of the unfolded protein response by lipid bilayer stress. Mol. Cell. 2017;67(4):673–684. PubMed PMID: 28689662. [PubMed] [Google Scholar]

26. Panzhinskiy E., Hua Y., Culver B., Ren J., Nair S. Endoplasmic reticulum stress upregulates protein tyrosine phosphatase 1B and impairs glucose uptake in cultured myotubes. Diabetologia. 2013;56(3):598–607. PubMed PMID: 23178931; PubMed Central PMCID: PMCPMC3568946. [PMC free article] [PubMed] [Google Scholar]

27. Ozcan U., Yilmaz E., Ozcan L., Furuhashi M., Vaillancourt E., Smith R.O. Chemical chaperones reduce ER stress and restore glucose homeostasis in a mouse model of type 2 diabetes. Science. 2006;313(5790):1137–1140. PubMed PMID: 16931765; PubMed Central PMCID: PMCPMC4741373. [PMC free article] [PubMed] [Google Scholar]

28. Hage Hassan R., Hainault I., Vilquin J.T., Samama C., Lasnier F., Ferre P. Endoplasmic reticulum stress does not mediate palmitate-induced insulin resistance in mouse and human muscle cells. Diabetologia. 2012;55(1):204–214. PubMed PMID: 22006247. [PubMed] [Google Scholar]

29. Zinszner H., Kuroda M., Wang X., Batchvarova N., Lightfoot R.T., Remotti H. CHOP is implicated in programmed cell death in response to impaired function of the endoplasmic reticulum. Genes Dev. 1998;12(7):982–995. Epub 1998/05/09. PubMed PMID: 9531536; PubMed Central PMCID: PMC316680. [PMC free article] [PubMed] [Google Scholar]

30. Schultze S.M., Hemmings B.A., Niessen M., Tschopp O. PI3K/AKT, MAPK and AMPK signalling: protein kinases in glucose homeostasis. Expert Rev. Mol. Med. 2012;14:e1. PubMed PMID: 22233681. [PubMed] [Google Scholar]

31. Patel S., Doble B., Woodgett J.R. Glycogen synthase kinase-3 in insulin and Wnt signalling: a double-edged sword? Biochem. Soc. Trans. 2004;32(Pt 5):803–808. PubMed PMID: 15494020; PubMed Central PMCID: PMCPMC4485494. [PMC free article] [PubMed] [Google Scholar]

32. Cagliani R., Fruguglietti M.E., Berardinelli A., D'Angelo M.G., Prelle A., Riva S. New molecular findings in congenital myopathies due to selenoprotein N gene mutations. J. Neurol. Sci. 2011;300(1–2):107–113. PubMed PMID: 20937510. [PubMed] [Google Scholar]

33. Maggi L., Scoto M., Cirak S., Robb S.A., Klein A., Lillis S. Congenital myopathies - clinical features and frequency of individual subtypes diagnosed over a 5-year period in the United Kingdom. Neuromuscul. Disord. 2013 Epub 2013/02/12. doi: S0960-8966(13)00009-6 [pii] 10.1016/j.nmd.2013.01.004. PubMed PMID: 23394784. [PubMed] [Google Scholar]

34. DeFronzo R.A., Tripathy D. Skeletal muscle insulin resistance is the primary defect in type 2 diabetes. Diabetes Care. 2009;32(Suppl 2):S157–S163. PubMed PMID: 19875544; PubMed Central PMCID: PMCPMC2811436. [PMC free article] [PubMed] [Google Scholar]

35. Pozzer D., Varone E., Chernorudskiy A., Schiarea S., Missiroli S., Giorgi C. A maladaptive ER stress response triggers dysfunction in highly active muscles of mice with SELENON loss. Redox Biol. 2018;20:354–366. PubMed PMID: 30391828. [PMC free article] [PubMed] [Google Scholar]

36. Deldicque L., Cani P.D., Philp A., Raymackers J.M., Meakin P.J., Ashford M.L. The unfolded protein response is activated in skeletal muscle by high-fat feeding: potential role in the downregulation of protein synthesis. Am. J. Physiol. Endocrinol. Metab. 2010;299(5):E695–E705. PubMed PMID: 20501874. [PubMed] [Google Scholar]

37. Chomentowski P., Coen P.M., Radikova Z., Goodpaster B.H., Toledo F.G. Skeletal muscle mitochondria in insulin resistance: differences in intermyofibrillar versus subsarcolemmal subpopulations and relationship to metabolic flexibility. J. Clin. Endocrinol. Metab. 2011;96(2):494–503. PubMed PMID: 21106709; PubMed Central PMCID: PMCPMC3048328. [PMC free article] [PubMed] [Google Scholar]

38. Song B., Scheuner D., Ron D., Pennathur S., Kaufman R.J. Chop deletion reduces oxidative stress, improves beta cell function, and promotes cell survival in multiple mouse models of diabetes. J. Clin. Investig. 2008;118(10):3378–3389. Epub 2008/09/09, PubMed PMID: 18776938; PubMed Central PMCID: PMC2528909. [PMC free article] [PubMed] [Google Scholar]

39. Oyadomari S., Koizumi A., Takeda K., Gotoh T., Akira S., Araki E. Targeted disruption of the Chop gene delays endoplasmic reticulum stress-mediated diabetes. J. Clin. Investig. 2002;109(4):525–532. PubMed PMID: 11854325; PubMed Central PMCID: PMCPMC150879. [PMC free article] [PubMed] [Google Scholar]

40. Ariyama Y., Shimizu H., Satoh T., Tsuchiya T., Okada S., Oyadomari S. Chop-deficient mice showed increased adiposity but no glucose intolerance. Obesity. 2007;15(7):1647–1656. PubMed PMID: 17636082. [PubMed] [Google Scholar]

41. Ball G., Demmerle J., Kaufmann R., Davis I., Dobbie I.M., Schermelleh L. SIMcheck: a toolbox for successful super-resolution structured illumination microscopy. Sci. Rep. 2015;5:15915. PubMed PMID: 26525406; PubMed Central PMCID: PMCPMC4648340. [PMC free article] [PubMed] [Google Scholar]

42. Fumagalli S., Fiordaliso F., Perego C., Corbelli A., Mariani A., De Paola M. The phagocytic state of brain myeloid cells after ischemia revealed by superresolution structured illumination microscopy. J. Neuroinflammation. 2019;16(1):9. PubMed PMID: 30651101; PubMed Central PMCID: PMCPMC6335825. [PMC free article] [PubMed] [Google Scholar]

43. Zito E., Chin K.T., Blais J., Harding H.P., Ron D. ERO1-beta, a pancreas-specific disulfide oxidase, promotes insulin biogenesis and glucose homeostasis. J. Cell Biol. 2010;188(6):[821]–[832]. Epub 2010/03/24. doi: jcb.200911086 [pii] 10.1083/jcb.200911086. PubMed PMID: 20308425; PubMed Central PMCID: PMC2845084. [PMC free article] [PubMed] [Google Scholar]
